Check for updates

ADVANCED ELECTRONIC MATERIALS
www.advelectronicmat.de

Local Characterization of Field Emission Properties of Graphene Flowers

Filippo Giubileo, Daniele Capista, Enver Faella, Aniello Pelella, Woo Young Kim, Paola Benassi, Maurizio Passacantando, and Antonio Di Bartolomeo**

An experimental study about field emission properties of commercially available graphene flowers cloth is reported. Material characterization by means of X-ray diffraction, Raman spectroscopy, and X-ray photoemission spectroscopy confirms the formation of high quality vertical few-layers graphene nanosheets. A tip-anode setup is exploited in which nanomanipulated tungsten tip is used as the anode at controlled distance from the emitter in order to reduce the effective emitting area below 1 μm^2, giving access to local characterization. A turn-on field as low as 0.07 V nm^{-1} and field enhancement factor up to 32 for very small cathode–anode separation distances is demonstrated, in the range 400–700 nm. It is also shown that the turn-on field increases for increasing distances, while the field enhancement factor decreases. Finally, time stability of the field emission current is reported, evidencing a reduction of the fluctuations for lower current levels.

1. Introduction

Field emission (FE) is a quantum phenomenon for which electrons can be extracted from a material favoring the tunneling through the vacuum potential barrier by the application of an electric field as strong as 10^7 V m^{-1}.[1] Therefore, FE-based devices have wide applicability in vacuum electronics, as flat-panel displays,[2,3] X-ray sources,[4] high-resolution electron beam instruments,[5] memories,[6] and microwave tubes.[7] In comparison with thermionic emission, FE has the great advantage to allow less power consumption, high emission current density, stability, and fast response time.

The need for high electric field to switch-on the cold electron emission triggered the interest of scientists toward the use of nanostructures to realize FE devices,[8,9] to profit from the huge aspect ratio that favors the local field enhancement in proximity of tips, protrusions, etc. Indeed, soon after their discovery by Iijima,[10] carbon nanotubes (CNTs) were identified as the prototype of nano-emitters.[11–14] Since then, an enormous number of one-dimensional nanostructures (nanowires,[15–18] nanorods,[19] nanopillars[20–22]) have been investigated as field emitters. As second milestone, the discovery of graphene by Geim and Novoselov[23] enlarged the interest toward the production of two-dimensional emitters considering the sharpness of nanosheet edges and also their suitability in planar device technology.

Graphene[24–26] and several other 2D materials[27] such as boron nitride,[28] black phosphorous,[29] MXenes,[30] and transition metal dichalcogenides (TMDs)[31–37] have been studied for their favorable FE properties including low turn-on voltage, time stability, and high current density. Furthermore, the tuning of FE properties in 2D materials by means of chemical-doping or gating has been reported.[38–40]

Due to the several beneficial properties for FE (atomically thick sheets, high carrier mobility, excellent mechanical strength and chemical stability), either graphene or reduced oxide graphene based devices have been fabricated by standard mechanical exfoliation, chemical vapor deposition, screen-printing or electrophoretic deposition.[41] Graphene-based FE devices have been realized using flakes lying on standard substrates such as Si/SiO_2 as well as to cover other systems including pillars or nanoparticles or tip arrays.[42,43]

On the other hand, to further improve the FE performance various strategy were implemented to obtain side edges well exposed, as in vertically aligned nanosheets or edges arrays, to increase the emission efficiency (by lowering the turn-on field, increasing the field enhancement factor or obtaining a higher current stability). As demonstrated for some TMDs (MoS_2,

F. Giubileo, E. Faella, A. Pelella, A. Di Bartolomeo
CNR-SPIN Salerno
via Giovanni Paolo II n. 132, Fisciano 84084, Italy
E-mail: filippo.giubileo@spin.cnr.it; adibartolomeo@unisa.it
D. Capista, P. Benassi, M. Passacantando
Department of Physical and Chemical Science
University of L'Aquila
via Vetoio, Coppito, L'Aquila 67100, Italy
E. Faella, A. Pelella, A. Di Bartolomeo
Physics Department "E. R. Caianiello"
University of Salerno and CNR-SPIN Salerno
via Giovanni Paolo II n. 132, Fisciano 84084, Italy
W. Y. Kim
Department of Electronic Engineering
Faculty of Applied Energy System
Jeju National University
Jeju Special Self-Governing Province, Jeju-si 63243, Korea
M. Passacantando
CNR-SPIN L'Aquila
via Vetoio, Coppito, L'Aquila 67100, Italy

The ORCID identification number(s) for the author(s) of this article can be found under https://doi.org/10.1002/aelm.202200690.

© 2022 The Authors. Advanced Electronic Materials published by Wiley-VCH GmbH. This is an open access article under the terms of the Creative Commons Attribution License, which permits use, distribution and reproduction in any medium, provided the original work is properly cited.

DOI: 10.1002/aelm.202200690

© 2022 The Authors. Advanced Electronic Materials published by Wiley-VCH GmbH

2199160x, 2023, 1, Downloaded from https://onlinelibrary.wiley.com/doi/10.1002/aelm.202200690 by Universita Di Salerno, Wiley Online Library on [10/01/2023]. See the Terms and Conditions (https://onlinelibrary.wiley.com/terms-and-conditions) on Wiley Online Library for rules of use; OA articles are governed by the applicable Creative Commons License

WS_2, WSe_2), for a given material the FE performance can be increased by the formation of nanoflowers,[44,45] structures characterized by abundant free edges with nanosized dimensions.[9] Nanocarbon films containing scrolled graphene structures and nanowalls grown by chemical vapor deposition have been investigated as field emitters in a parallel plate configuration, reporting low threshold field of 1–2 V μm^{-1}.[46]

In this paper, we report the FE characterization of flower-like graphene nanostructures having numerous thin free edges in the vertical direction. Profiting of the high carrier mobility and the high aspect ratio of the graphene edges, excellent field emission characteristics are expected because the surface structure is suitable for a strong enhancement of the local electric field, favoring the electron extraction. We use a tip-anode setup realized inside a scanning electron microscope to allow precise positioning of the anode in close proximity of the emitting surface, in the range of hundreds of nanometers. The dependence of the main performance parameters, such as turn-on field and field enhancement factor, on the cathode–anode separation distance is experimentally investigated.

2. Experimental Section

Commercially available graphene flowers (by Incubation Alliance) were investigated for their use as field emitters. Woven graphene flower cloth is a three-dimensional composite material with densely formed graphene on the surface of the carbon fiber.[47] All the surface of the carbon fibers is covered by independently formed graphene. The result is a 3D structure with vertically oriented graphene edges on carbon fiber, as shown in **Figure 1**a. Structural characterization of the graphene flowers as well as elemental analysis was performed in order to confirm the high quality of graphene samples. A room temperature micro-Raman spectrometer (LABRAM, Horiba-Jobin Yvon) equipped with an optical microscope (Olympus SLMPLAN 20× objective) was used to acquire Raman spectra using a 532 nm diode-pumped solid state laser (0.1 mW) with a spot size of 1 μm. Figure 1b shows the Raman spectrum of graphene flowers, in the frequency range 1200–2900 cm^{-1}, in which the presence of two prominent peaks at 1576.9 and 2690.6 cm^{-1}, and two small peaks at 1348.3 and 2444.3 cm^{-1}

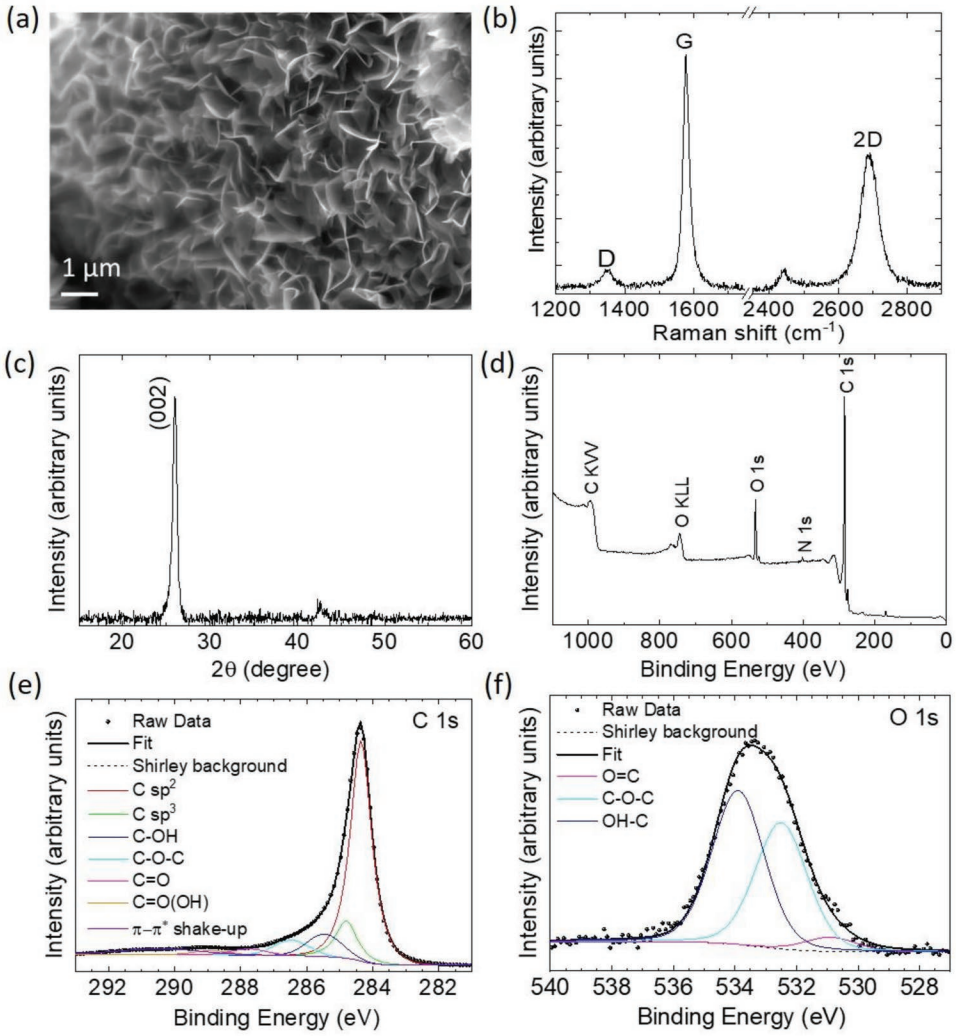

Figure 1. a) SEM image of graphene flower sample. b) Raman spectrum. c) XRD pattern. d) XPS survey spectrum. e) C 1s core level deconvolution. f) O 1s core level deconvolution.

© 2022 The Authors. Advanced Electronic Materials published by Wiley-VCH GmbH

2199160x, 2023, 1, Downloaded from https://onlinelibrary.wiley.com/doi/10.1002/aelm.202200690 by Universita Di Salerno, Wiley Online Library on [10/01/2023]. See the Terms and Conditions (https://onlinelibrary.wiley.com/terms-and-conditions) on Wiley Online Library for rules of use; OA articles are governed by the applicable Creative Commons License

is observed. The G-band peak positioned at 1576.9 cm^{-1} corresponds to the first-order scattering of the E_{2g} phonons (i.e., in-plane bond-stretching motion of pairs of C sp^2 atoms), while the 2D-band peak located at 2690.6 cm^{-1} corresponds to transversal optical phonon mode occurring near the corners of the first Brillouin zone. The position of the 2D peak is much lower than 2725 cm^{-1} expected for graphite, confirming that few-layer graphene nanosheets were successfully obtained. Moreover, the small D-peak at 1348.3 cm^{-1} indicates that the graphene flowers are of good quality, with a low defect density. Finally, the peak at 2444.3 cm^{-1} is associated to D + D'' (a combination of a D phonon and an acoustic longitudinal phonon, D''). It was noticed that the Raman spectrometer was calibrated by using two reference samples, namely the Si and the HOPG.

The X-ray diffraction (XRD) measurements were performed by means of Bruker D5000 diffractometer with Cu Kα ($\lambda = 1.5418$ Å) radiation in Bragg–Brentano geometry. The XRD pattern is shown in Figure 1c and it is characterized by a narrow diffraction peak at $2\theta = 26°$ which corresponds to the carbon graphite (002) reflection of the hexagonal. A second smaller peak is observed at about 43° that can be assigned to the (100) peak, another characteristic peak expected for the diffraction of graphenes. The Bragg's law states that the distance d between successive layers of atoms is given by $d(hkl) = \lambda/2\sin\theta$ therefore the lattice constant of the primitive cell can be derived as $c = 2d$. In this case a lattice constant $c = 0.6849$ nm is obtained which corresponds to an increase of about 0.9% respect to the value of a graphite (JCPDS 075-1621). Anyway, XRD confirms that the crystalline order of multi-layer graphene flowers was preserved.

The elemental composition of graphene flowers was also analyzed by X-ray photoelectron spectroscopy (XPS), for a better understanding of the surface chemical states. XPS experiments were performed at a base pressure of 10^{-10} mbar by means of a PHI-1257 system equipped with a hemispherical analyzer. Nonmonochromatic Mg Kα X-ray source ($h\nu = 1253.6$ eV) was used to irradiate the sample under study. The values of binding energy (BE) were normalized with respect the position of the C 1s peak, while all core levels were fitted with Gaussian functions, considering a Shirley background. Figure 1d shows a survey spectrum in the range 0–1100 eV, where the main contributions are identified as carbon (C 1s), oxygen (O 1s), and corresponding Auger signals (C KVV and O KLL). The C 1s core level (Figure 1e) can be de-convoluted by several contributions, namely the dominant C=C (sp^2) bond (at 284.4 eV), with minor contributions from the C–C (sp^3) at 284.8 eV, C–OH (at 285.5 eV), C–O–C (at 286.5 eV), C=O (at 287.8 eV), C=O(OH) (at 288.9 eV), and π–π^* shake-up (at 290.4 eV). It was noticed that the peaks related to the oxidized carbon species were very weak. The O1s peak is reported in Figure 1f, evidencing the contributions from OH–C (at 533.9 eV), O–C (at 532.5 eV), and small signature of O=C (at 530.9 eV). Considering the XPS results from which functional groups of carbon are present, it allows to justify the very slight increase in the lattice constant c (see the XRD data) due precisely to the presence of them between adjacent graphene planes.

2.1. Field Emission Characterization

The field emission characterization was performed inside the vacuum chamber of a scanning electron microscope (SEM, Zeiss LEO 1430) at pressure of 10^{-6} Torr. Anode was used as an electrochemically etched tungsten tip, with curvature radius of about 100 nm, mounted on a nano-manipulator (MM3A by Kleindiek) that allows a precise positioning with step resolution of about 5 nm with respect the sample material (cathode). Electrical measurements were realized by connecting anode and cathode tips (by triaxial vacuum feedthroughs) to a source-measurement unit (Keithley 4200): A bias sweep up to +120 V can be applied on the anode while grounding the cathode (larger bias is avoided to prevent high voltage failure of electronic controller of the piezo-driven probes); the FE current flowing between anode and cathode is measured with a precision better than 0.1 pA. A schematic of the setup for the electrical measurements is shown in **Figure 2**a. As initial step, both tips are approached on the sample surface to verify the electrical contact and estimate the total series resistance of circuit. Figure 2b shows a current–voltage (I–V) measurement performed in this configuration demonstrating the good ohmic contact formed between the tips and the sample and a series resistance of about 250 kΩ.

Soon after, the configuration for FE measurements is easily obtained by retracting the anode tip at controlled distance d from the sample surface. For what concerns the cathode–anode

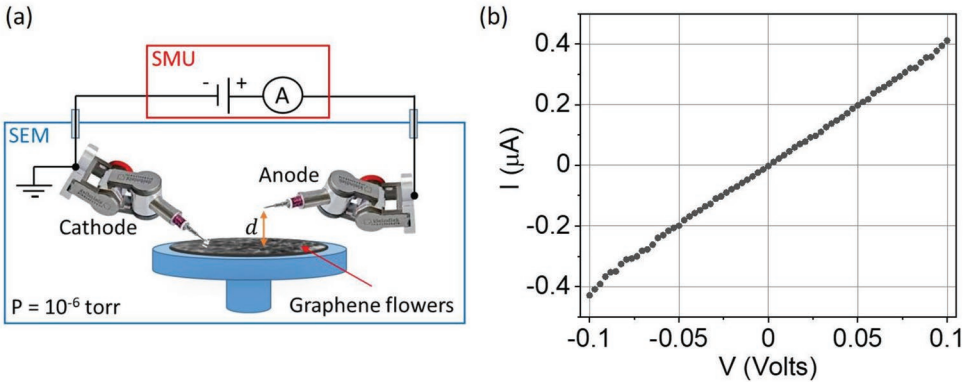

Figure 2. a) Schematic of the experimental setup for FE measurements with the tip-anode represented at controlled distance d from the emitting surface (grounded cathode). b) I–V characteristic measured with both tips contacting the surface.

© 2022 The Authors. Advanced Electronic Materials published by Wiley-VCH GmbH

2199160x, 2023, 1, Downloaded from https://onlinelibrary.wiley.com/doi/10.1002/aelm.202200690 by Universita Di Salerno, Wiley Online Library on [10/01/2023]. See the Terms and Conditions (https://onlinelibrary.wiley.com/terms-and-conditions) on Wiley Online Library for rules of use; OA articles are governed by the applicable Creative Commons License

separation distance, it is directly measured inside the scanning electron microscope (that is typically calibrated with reference grids) by imaging. In particular, the system tip-sample is installed on a rotating stage to position the FE device with the current channel (vacuum gap between cathode and anode) almost perpendicular to the electron beam for precise measurement. A flat gold plate was used as cathode (emitter) for identifying the floor noise of the experimental setup (typically of the order of 10^{-13} A).

The FE setup that exploits a tip-shaped anode has the great advantage to allow a local characterization of the FE properties of the emitting cathode. If it is assumed that the material has a uniform work function, the distance from the emitting sites of the anode electrode is extremely relevant, because the tunneling phenomenon that is used has an exponential dependence on the cathode–anode separation distance. The FE experiments were commonly analyzed within the theoretical framework by Fowler and Nordheim (FN theory).[48] Despite the very simple model that considers an ideal gas of free electron (a Sommerfeld-type metal) at $T = 0$ K, a planar cathode with uniform work-function over all the surface, and uniform electric field perpendicular to the emitting surface, the FN theory provides an analytical expression (Equation (1)) for the FE current density as a function of the externally applied electric field:

$$I = \mathrm{S} \cdot a \frac{E_{\mathrm{local}}^2}{\phi} \cdot e^{\left[-b\frac{\phi^{3/2}}{E_{\mathrm{local}}}\right]} \quad (1)$$

where S is the emitting area, $a = 15.4 \times 10^{-7}$ V^{-2} A eV, and $b = 68.3 \times 10^{6}$ eV$^{-3/2}$ cm^{-1} V are constants; φ is the work function of the emitting material; $E_{\mathrm{local}} = \beta d^{-1} V$ is the local electric field caused by a potential difference V when the cathode and anode are separated by a distance d, considering the field enhancement factor β that takes into account the local amplification of the field due to the emitter geometry.

Importantly, this model was widely used as a successful first approximation approach to analyze FE experimental data in almost all kind of experiments, from planar to nanostructured surfaces, either metals or semiconductors, networks, arrays, etc.[49,50] For the sake of completeness, it is mentioned here that several models were also reported to generalize the FN theory to more complicated scenarios. For instance, corrections can be introduced to take into account non-uniform work-function or field enhancement factor as well as the presence of curved surfaces, non-zero temperature, etc.[51–54]

As mentioned before, the use of a metallic tip-shaped anode allows to get local field emission information, indeed only electrons emitted from a small area will contribute to the total FE current, while the standard parallel plate setup employs anode with area up to several mm^2.

Comsol Multiphysics simulation software was used to calculate the electric field distribution generated by a conical tip (positively biased with +100 V) with curvature radius of 100 nm and positioned 500 nm far away from a grounded planar cathode emitter. The resulting electric field is represented in **Figure 3**a as a color map. The intensity of the electric field on the cathode surface can be plotted and as expected it was found that the field is higher in correspondence of the tip axis and it reduces by moving away from the axis, as shown in Figure 3b. The computation was performed with a resolution step $\Delta r = 20$ nm.

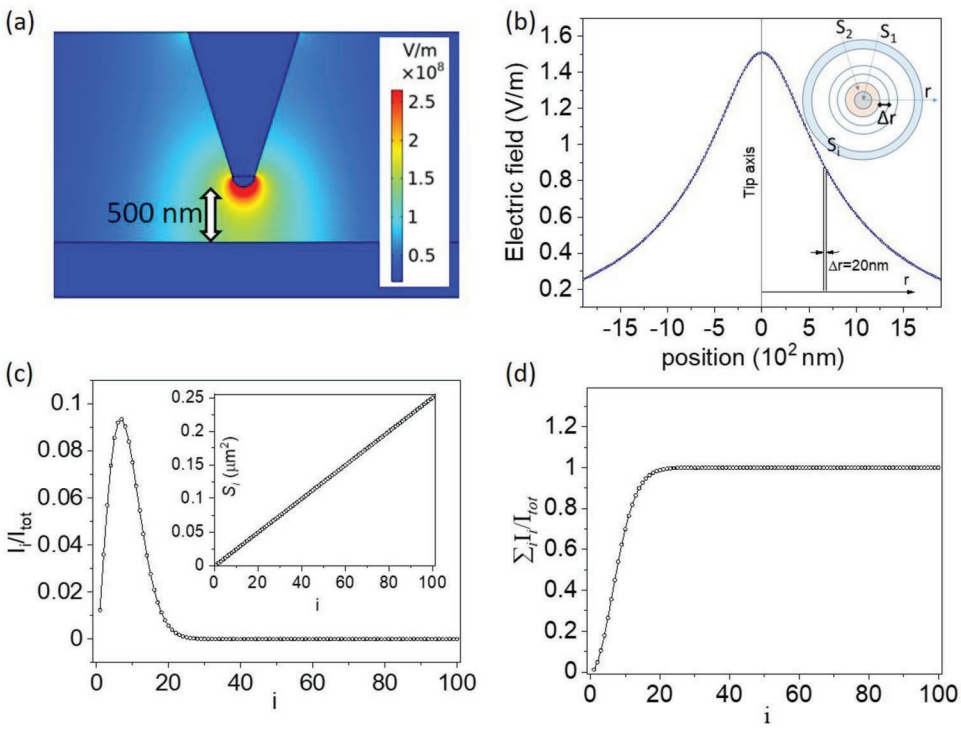

Figure 3. a) Electric field simulation assuming a metallic tip biased with +100 V and positioned 500 nm above the planar surface of the cathode. b) Electric field profile at the cathode surface. The position is measured with respect the tip axis. In the inset: cathode surface divided in a series of concentric rings of width $\Delta r = 20$ nm. c) Relative contribution to the total current from each surface element S_i. In the inset: dependence of S_i on i index. d) Cumulative plot: for each i the plot gives the total current resulting by summing the contributions from all the j rings corresponding at $j \leq i$.

© 2022 The Authors. Advanced Electronic Materials published by Wiley-VCH GmbH

2199160x, 2023, 1, Downloaded from https://onlinelibrary.wiley.com/doi/10.1002/aelm.202200690 by Universita Di Salerno, Wiley Online Library on [10/01/2023]. See the Terms and Conditions (https://onlinelibrary.wiley.com/terms-and-conditions) on Wiley Online Library for rules of use; OA articles are governed by the applicable Creative Commons License

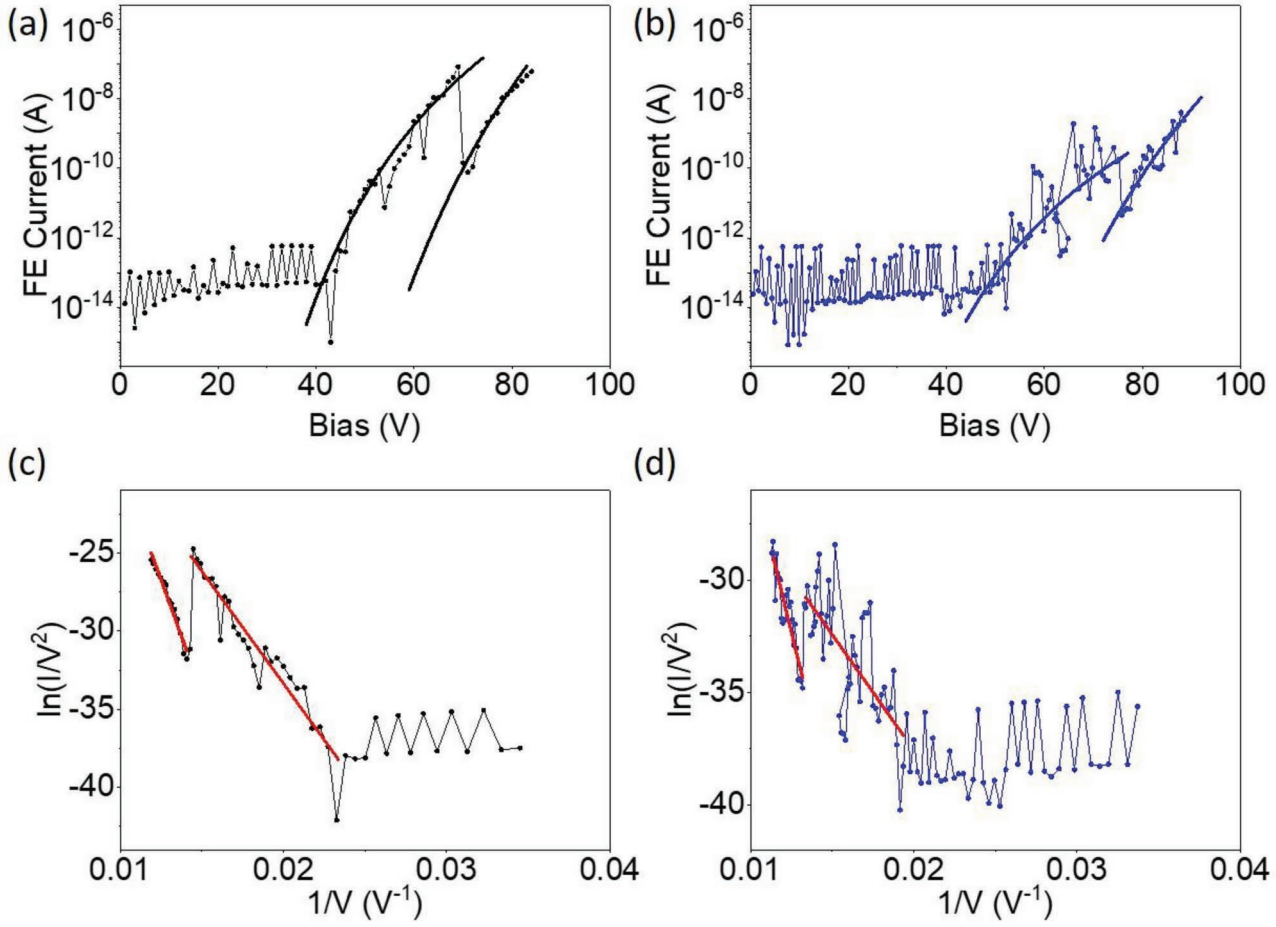

Figure 4. a,b) FE characteristics measured in two different locations of the sample. Experimental data are reported as scattered graphs and they are compared to the expected Fowler–Nordheim behavior of Equation (1) (solid lines). c,d) Corresponding FN-plots with linear fits of the two current raise regions, before and after the current drop.

So the emitting area can be divided in a series of concentric rings of fixed width ($\Delta r = 20$ nm) with surface area

$$S_i = \pi\left((\Delta r \cdot i)^2 - (\Delta r \cdot (i-1))^2\right) \quad (2)$$

Each element of cathode area S_i will contribute to the FE current according to the FN formula reported in Equation (1), where the electric field for each element of area will be given by the field profile calculated before. Consequently, the total current I_{tot} can be calculated as

$$I_{tot} = \sum_i I_i \quad (3)$$

where I_i is the FE current due to the i-element with surface area S_i on which the electric field is given by the distribution reported in Figure 3b. Each contribution I_i can be calculated and plotted as I_i/I_{tot} in Figure 3c.

It was noticed that the current contribution depends on S_i that is a linearly increasing function of i (see inset in Figure 3b); at the same time, increasing i, the intensity of the electric field decreases, because it is increasing the distance from the anode axis. As a result, the I_i/I_{tot} is non-monotonous with a maximum, due to the competitive effect due to the S_i value increasing for larger index i, while the electric field decreases.

Finally, by computing the total current I_{tot} collected at the anode it was noticed that it is a saturating function of the index i. Figure 3d shows that almost all FE current (99.9%) is emitted from the rings for $i \leq 25$ that corresponds to a circular area with radius $R = 25 \cdot \Delta r = 500$ nm, i.e., an area of about 0.8 μm^2.

FE measurements on graphene flowers were performed at room temperature inside the SEM chamber at a pressure of 10^{-6} mbar, initially positioning the anode tip at 400 nm from the sample surface (cathode contacted by the second tip). **Figure 4** demonstrates two examples of FE characteristics measured by sweeping the bias on the anode from 0 V up to +80 V, with grounded cathode. The I–V curves shown in Figure 4a,b were measured in two different locations of the same sample. It was noticed that in both cases the FE current is unstable with important drops followed by new raising of the current. In particular, in Figure 4a, the current remains at the floor noise level of the measurement setup (about 0.1 pA) for bias up to 40 V. Only for larger bias, the current start to flow through the vacuum and electrons is collected at the tip

© 2022 The Authors. Advanced Electronic Materials published by Wiley-VCH GmbH

2199160x, 2023, 1, Downloaded from https://onlinelibrary.wiley.com/doi/10.1002/aelm.202200690 by Universita Di Salerno, Wiley Online Library on [10/01/2023]. See the Terms and Conditions (https://onlinelibrary.wiley.com/terms-and-conditions) on Wiley Online Library for rules of use; OA articles are governed by the applicable Creative Commons License

anode. Experimental data (scattered plots in Figure 4a,b) are compared to the FN-theory expectation (solid lines according to Equation (1)). The current increases exponentially (the plot being reported in semi-log scale), up to six order of magnitudes in a small bias range (up to about 60 V). This current raise is followed by a sudden drop at about 62 V, and then by a new current raise, again according to the FE behavior predicted by the FN theory. Similar behavior is reported also in Figure 4b for measurement performed in a different location. Such unstable behavior of the FE current has been often observed when performing initial electrical sweep on emitter virgin areas. However, the measurement itself has a positive conditioning effect in stabilizing the emitter behavior. Indeed, one of the main responsible of the instabilities is the presence of adsorbates on the cathode surface.[55–57] They can cause either local increase of field enhancement factor (the adsorbate represent a localized protrusion where the field is enhanced) or reduction of local work function favoring an early switch-on of the emission. The conditioning effect is mostly due to the desorption of adsorbates that happens when local temperature became very high for Joule heating. It was noticed that the curves after the conditioning show similar slopes indicating that the clean surface has similar work function in different locations, as expected. Moreover, when dealing with nanoflowers, it can also happen that individual nanosheet protrudes more than others. In such a case it behaves like a protrusion: the FE current starts in this location due to the reduced cathode–anode separation and to the field enhancement; however, for increasing bias, the current density can become too high causing the burning of the protruding nanosheet, while the overall morphology of the cathode remains unaltered. The observed current drops typically correspond to these burning/desorption events and they are not anymore present after the conditioning produced by the first electrical sweep. It was reported also for doped single-walled nanotubes that an increase of the threshold field with respect to pristine nanotubes is mostly due to the removal of nanotubes with smallest diameters, while the work function at the apexes remains almost unaltered.[58] The second current rump up is still the result of the FE phenomenon, but in a more stable configuration in which adsorbates and/or

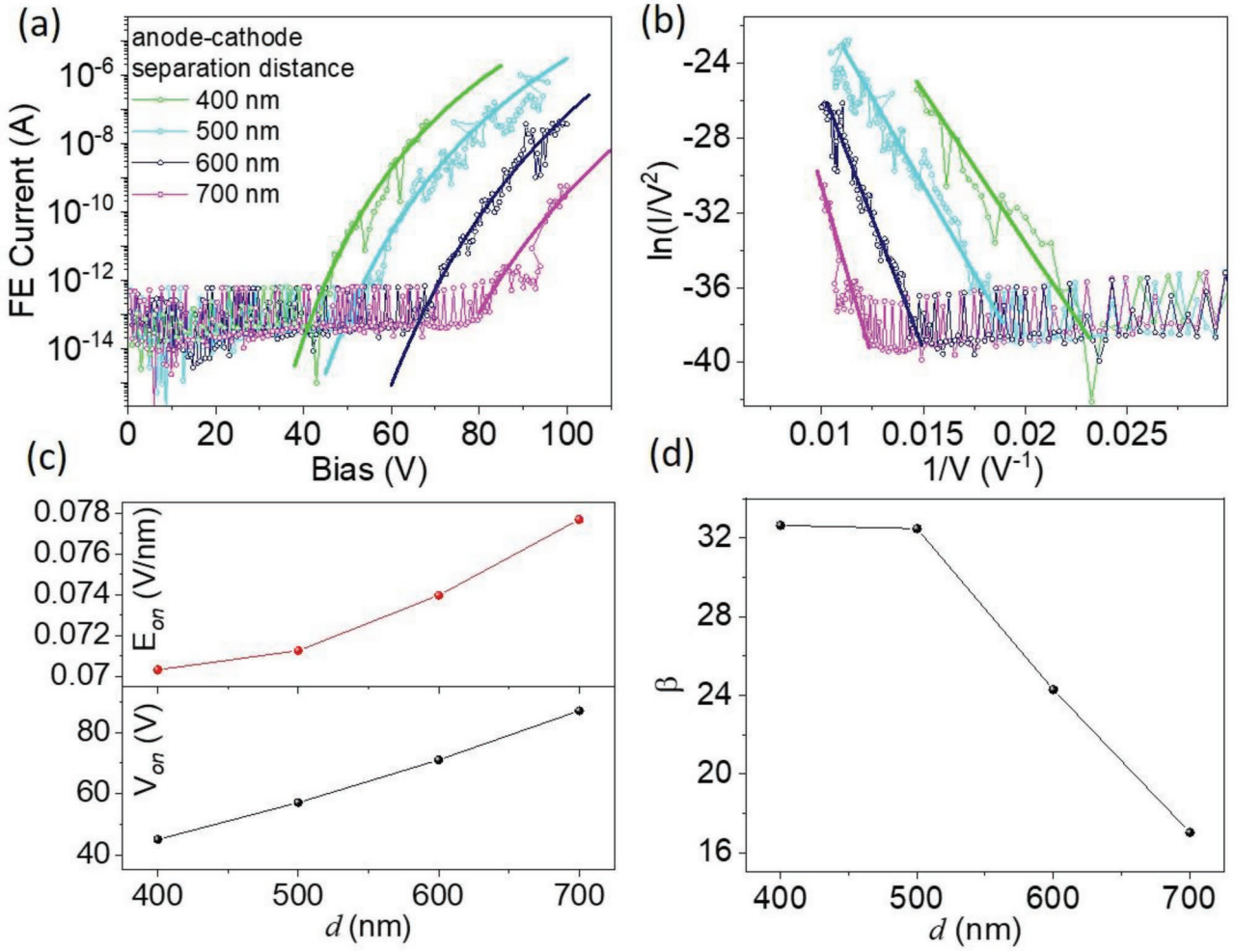

Figure 5. a) FE characteristics measured in a fixed location on the sample surface for different values of the anode–cathode separation distance in the range 400–700 nm, and the corresponding b) FN plots. c) Turn-on voltage (bottom plot), turn-on field (top plot), and d) field enhancement factor, extracted from experimental data and fittings, as function of the separation distance *d*.

© 2022 The Authors. Advanced Electronic Materials published by Wiley-VCH GmbH

2199160x, 2023, 1, Downloaded from https://onlinelibrary.wiley.com/doi/10.1002/aelm.202200690 by Universita Di Salerno, Wiley Online Library on [10/01/2023]. See the Terms and Conditions (https://onlinelibrary.wiley.com/terms-and-conditions) on Wiley Online Library for rules of use; OA articles are governed by the applicable Creative Commons License

protruding nanosheets have been removed. The second ramp corresponds to an increased turn-on voltage was noticed. As a confirmation, Figure 4c,d shows the FN plots corresponding to the FE curves in Figure 4a,b, respectively. Indeed, these plots are typically used to confirm the FE nature of the measured I–V characteristics. In particular, from Equation (1) it turns out that $\ln(I/V^2) \propto 1/V$ (the so-called FN plot) should be linear. It was noticed that in both cases, the two successive current raises have a linear FN plot, confirming that the device is in the FE regime before and after the current drop. Moreover, it was observed that after the conditioning effect (i.e., after the current drop), the FN plots become less noisy, confirming the increased stability of the device.

In the following, the reported experimental data in the FE regime have been always measured after a complete conditioning process to obtain stable and repeatable I–V characteristics. The FE curves reported in **Figure 5**a are measured in a fixed sample location, by varying the cathode–anode separation distance in the range 400–700 nm. All curves are compared to the theoretical expectation according to Equation (1) (solid lines). For each curve, the turn-on voltage V_{on} (here defined as the voltage needed to have an emitted current of 1 pA) and the corresponding turn-on field E_{on} that can be calculated as $E_{on} = V_{on} \cdot (\beta/d)/k_{tip}$ can be extracted, where β is the field enhancement factor and k_{tip} is the correction factor that takes into account the tip shaped anode.[59] It was noticed that V_{on} increased monotonously by increasing d , from a minimum value of 45 V at d = 400 nm up to about 85 V at d = 700 nm. The factor β is obtained from the slope m of the FN plots (Figure 5b), according to the formula $\beta = (bd\phi^{3/2}) \cdot k_{tip}/m$. Then, the turn-on field is easily estimated to monotonously increase in the range 0.070–0.078 V nm^{-1}. The dependence of the turn-on voltage (and field) on the distance d is summarized in Figure 5c. Similarly, it was obtained that the field enhancement factor in this distance range is a decreasing function of d, from a maximum value of about 33 at d = 400 nm down to 16 for d = 700 nm, as shown in Figure 5d. At higher distances, the cathode appears flatter and the enhancement factor decreases.

Finally, the stability of the device by monitoring the FE current over time was tested, an important parameter toward the exploitation of emitters in technological applications.[60,61] The FE stability of graphene flowers has been checked by positioning the anode at fixed distance from the surface, by applying a constant bias and measuring the FE current versus time. In **Figure 6**a, the measurement performed at d = 500 nm at a constant bias of 80 V is shown. The measured current has a mean value of 31 nA, with large fluctuations around the mean level. From the statistical analysis of the experimental data, it was obtained that the standard deviation of the current values is 28 nA. The measurement by reducing the fixed voltage at 70 V was repeated. The current fluctuations were reduced, the measured current having a mean value of 1.1 nA and a standard deviation of 0.4 nA.

To compare the performance of graphene flowers as field emitters, their behavior can be compared in terms of turn-on field with other nanostructures which was previously characterized by using the same experimental setup. It was noticed that graphene flowers are more efficient as emitters allowing lower turn-on field (0.07 V nm^{-1}) with respect graphene flakes (0.6 V nm^{-1}),[42] carbon nanotubes networks (0.14 V nm^{-1}),[13] and InP nanoparticles covered by graphene layer (0.1 V nm^{-1}).[43] Similar turn-on field was achieved for MoS_2 nanoflowers (0.07–0.08 V nm^{-1}).[44]

3. Conclusions

We investigated the field emission properties of graphene flowers cloth. To access the local properties, i.e., from areas below 1 μm^2 we used an experimental setup inside a scanning electron microscope exploiting a nanomanipulated tip-shaped anode that allows the positioning in the order of hundreds of nanometres from the emitter surface. We report that initial electrical sweep has a conditioning effect in stabilizing the emitter behavior. We demonstrate a turn-on field as low as 0.07 V nm^{-1} for a cathode anode separation distance of 400 nm.

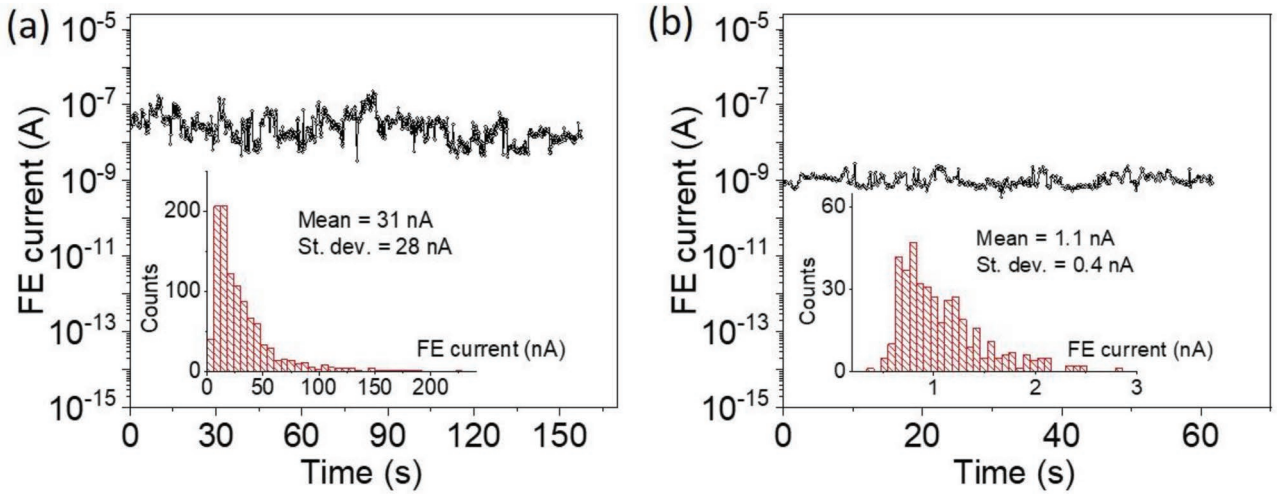

Figure 6. a) FE current stability measured at fixed bias of 80 V and the anode positioned 500 nm above the surface. In the inset, the histogram of the current values recorded during the current monitoring. b) FE current stability measured by reducing the bias to 70 V.

© 2022 The Authors. Advanced Electronic Materials published by Wiley-VCH GmbH

2199160x, 2023, 1, Downloaded from https://onlinelibrary.wiley.com/doi/10.1002/aelm.202200690 by Universita Di Salerno, Wiley Online Library on [10/01/2023]. See the Terms and Conditions (https://onlinelibrary.wiley.com/terms-and-conditions) on Wiley Online Library for rules of use; OA articles are governed by the applicable Creative Commons License

We show that by increasing the distance, the electric field to switch on the emission increases monotonously in the range 400–700 nm. We finally prove that the graphene flowers have good time stability that can be improved if working at reduced current levels of the order of nA.

Conflict of Interest

The authors declare no conflict of interest.

Data Availability Statement

The data that support the findings of this study are available from the corresponding author upon reasonable request.

Keywords

field emission, field enhancement factor, Fowler–Nordheim theory, graphene, turn-on field

Received: June 21, 2022
Revised: October 10, 2022
Published online: November 15, 2022

[1] K. L. Jensen, *Introduction to the Physics of Electron Emission*, 1st ed., John Wiley & Sons, Inc., Hoboken, NJ **2017**.
[2] Y. Zhao, Y. Chen, G. Zhang, R. Zhan, J. She, S. Deng, J. Chen, *Nanomaterials* **2021**, *11*, 240.
[3] Z. Chen, F. Zhu, Y. Wei, K. Jiang, L. Liu, S. Fan, *Nanotechnology* **2008**, *19*, 135703.
[4] B. Diop, V. T. Binh, *Rev. Sci. Instrum.* **2012**, *83*, 094704.
[5] F. Houdellier, G. M. Caruso, S. Weber, M. Kociak, A. Arbouet, *Ultramicroscopy* **2018**, *186*, 128.
[6] A. Di Bartolomeo, H. Rücker, P. Schley, A. Fox, S. Lischke, K.-Y. Na, *Solid-State Electron.* **2009**, *53*, 644.
[7] K. B. K. Teo, E. Minoux, L. Hudanski, F. Peauger, J.-P. Schnell, L. Gangloff, P. Legagneux, D. Dieumegard, G. A. J. Amaratunga, W. I. Milne, *Nature* **2005**, *437*, 968.
[8] F. Giubileo, A. Di Bartolomeo, L. Iemmo, G. Luongo, F. Urban, *Appl. Sci.* **2018**, *8*, 526.
[9] X. Fang, Y. Bando, U. K. Gautam, C. Ye, D. Golberg, *J. Mater. Chem.* **2008**, *18*, 509.
[10] S. Iijima, *Nature* **1991**, *354*, 56.
[11] J.-M. Bonard, K. A. Dean, B. F. Coll, C. Klinke, *Phys. Rev. Lett.* **2002**, *89*, 197602.
[12] M. Passacantando, F. Bussolotti, S. Santucci, A. Di Bartolomeo, F. Giubileo, L. Iemmo, A. M. Cucolo, *Nanotechnology* **2008**, *19*, 395701.
[13] F. Giubileo, L. Iemmo, G. Luongo, N. Martucciello, M. Raimondo, L. Guadagno, M. Passacantando, K. Lafdi, A. Di Bartolomeo, *J. Mater. Sci.* **2017**, *52*, 6459.
[14] R. Maheswaran, B. P. Shanmugavel, *J. Electron. Mater.* **2022**, *51*, 2786.
[15] M. Akbari-Saatlu, M. Procek, C. Mattsson, G. Thungström, H.-E. Nilsson, W. Xiong, B. Xu, Y. Li, H. H. Radamson, *Nanomaterials* **2020**, *10*, 2215.
[16] F. Giubileo, A. Di Bartolomeo, L. Iemmo, G. Luongo, M. Passacantando, E. Koivusalo, T. Hakkarainen, M. Guina, *Nanomaterials* **2017**, *7*, 275.
[17] F. Giubileo, A. D. Bartolomeo, Y. Zhong, S. Zhao, M. Passacantando, *Nanotechnology* **2020**, *31*, 475702.
[18] F. Giubileo, E. Faella, A. Pelella, A. Kumar, D. Capista, M. Passacantando, S. S. Kim, A. Di Bartolomeo, *Adv. Electron. Mater.* **2022**, *8*, 2200237.
[19] Z. Li, W. Wang, S. Deng, N. Xu, In *2005 International Vacuum Nanoelectronics Conference*, IEEE, USA **2005**, p. 9.
[20] A. Grillo, J. Barrat, Z. Galazka, M. Passacantando, F. Giubileo, L. Iemmo, G. Luongo, F. Urban, C. Dubourdieu, A. Di Bartolomeo, *Appl. Phys. Lett.* **2019**, *114*, 193101.
[21] F. Giubileo, M. Passacantando, F. Urban, A. Grillo, L. Iemmo, A. Pelella, C. Goosney, R. LaPierre, A. Di Bartolomeo, *Adv. Electron. Mater.* **2020**, *6*, 2000402.
[22] D. Yeşilpınar, C. Çelebi, *J. Vac. Sci. Technol., B* **2017**, *35*, 041801.
[23] K. S. Novoselov, *Science* **2004**, *306*, 666.
[24] J. Deng, R. Zheng, Y. Yang, Y. Zhao, G. Cheng, *Carbon* **2012**, *50*, 4732.
[25] A. Di Bartolomeo, F. Giubileo, L. Iemmo, F. Romeo, S. Russo, S. Unal, M. Passacantando, V. Grossi, A. M. Cucolo, *Appl. Phys. Lett.* **2016**, *109*, 023510.
[26] Y. Gao, S. Okada, *Carbon* **2019**, *142*, 190.
[27] A. Di Bartolomeo, *Nanomaterials* **2020**, *10*, 579.
[28] K. N. Yun, Y. Sun, J. S. Han, Y.-H. Song, C. J. Lee, *ACS Appl. Mater. Interfaces* **2017**, *9*, 1562.
[29] S. R. Suryawanshi, M. A. More, D. J. Late, *J. Vac. Sci. Technol., B: Nanotechnol. Microelectron.: Mater., Process., Meas., Phenom.* **2016**, *34*, 041803.
[30] B. Yang, J. Chen, X. Wu, B. Liu, L. Liu, Y. Tang, X. Yan, *Nanoscale* **2021**, *13*, 7622.
[31] L. Iemmo, F. Urban, F. Giubileo, M. Passacantando, A. Di Bartolomeo, *Nanomaterials* **2020**, *10*, 106.
[32] F. Giubileo, L. Iemmo, M. Passacantando, F. Urban, G. Luongo, L. Sun, G. Amato, E. Enrico, A. Di Bartolomeo, *J. Phys. Chem. C* **2019**, *123*, 1454.
[33] P. R. Dusane, B. R. Thombare, P. K. Bankar, G. Lole, D. Gavhane, C. V. Khedkar, B. Nagrare, A. Salunkhe, P. Kolhe, R. J. Choudhary, D. M. Phase, M. A. More, S. I. Patil, *Mater. Res. Bull.* **2019**, *116*, 67.
[34] F. Urban, M. Passacantando, F. Giubileo, L. Iemmo, A. Di Bartolomeo, *Nanomaterials* **2018**, *8*, 151.
[35] A. Di Bartolomeo, A. Pelella, F. Urban, A. Grillo, L. Iemmo, M. Passacantando, X. Liu, F. Giubileo, *Adv. Electron. Mater.* **2020**, *6*, 2000094.
[36] C. S. Rout, P. D. Joshi, R. V. Kashid, D. S. Joag, M. A. More, A. J. Simbeck, M. Washington, S. K. Nayak, D. J. Late, *Appl. Phys. Lett.* **2014**, *105*, 043109.
[37] A. Di Bartolomeo, A. Grillo, F. Giubileo, L. Camilli, J. Sun, D. Capista, M. Passacantando, *J. Phys. D: Appl. Phys.* **2020**, *54*, 105302.
[38] A. Di Bartolomeo, F. Urban, M. Passacantando, N. McEvoy, L. Peters, L. Iemmo, G. Luongo, F. Romeo, F. Giubileo, *Nanoscale* **2019**, *11*, 1538.
[39] A. Patra, M. A. More, D. J. Late, C. S. Rout, *J. Mater. Chem. C* **2021**, *9*, 11059.
[40] A. Pelella, A. Grillo, F. Urban, F. Giubileo, M. Passacantando, E. Pollmann, S. Sleziona, M. Schleberger, A. Di Bartolomeo, *Adv. Electron. Mater.* **2021**, *7*, 2000838.
[41] X. Wang, Y. Shi, In *Nanoscience & Nanotechnology Series* (Eds.: G. Zhang, N. Manjooran), Royal Society of Chemistry, Cambridge **2014**, p. 1.
[42] S. Santandrea, F. Giubileo, V. Grossi, S. Santucci, M. Passacantando, T. Schroeder, G. Lupina, A. Di Bartolomeo, *Appl. Phys. Lett.* **2011**, *98*, 163109.
[43] L. Iemmo, A. Di Bartolomeo, F. Giubileo, G. Luongo, M. Passacantando, G. Niu, F. Hatami, O. Skibitzki, T. Schroeder, *Nanotechnology* **2017**, *28*, 495705.

© 2022 The Authors. Advanced Electronic Materials published by Wiley-VCH GmbH

2199160x, 2023, 1, Downloaded from https://onlinelibrary.wiley.com/doi/10.1002/aelm.202200690 by Universita Di Salerno, Wiley Online Library on [10/01/2023]. See the Terms and Conditions (https://onlinelibrary.wiley.com/terms-and-conditions) on Wiley Online Library for rules of use; OA articles are governed by the applicable Creative Commons License

[44] F. Giubileo, A. Grillo, M. Passacantando, F. Urban, L. Iemmo, G. Luongo, A. Pelella, M. Loveridge, L. Lozzi, A. Di Bartolomeo, *Nanomaterials* **2019**, *9*, 717.
[45] Z. Li, J. Ma, Y. Zhou, Z. Yin, Y. Tang, Y. Ma, D. Wang, *Electrochim. Acta* **2018**, *283*, 306.
[46] V. I. Kleshch, D. A. Bandurin, P. Serbun, R. R. Ismagilov, D. Lützenkirchen-Hecht, G. Müller, A. N. Obraztsov, *Phys. Status Solidi B* **2018**, *255*, 1700270.
[47] https://incu-alliance.co.jp/english/graphene-flower-cloth/, .
[48] R. H. Fowler, L. Nordheim, *Proc. R. Soc. A* **1928**, *119*, 173.
[49] J.-M. Bonard, N. Weiss, H. Kind, T. Stöckli, L. Forró, K. Kern, A. Châtelain, *Adv. Mater.* **2001**, *13*, 184.
[50] F. Giubileo, A. D. Bartolomeo, A. Scarfato, L. Iemmo, F. Bobba, M. Passacantando, S. Santucci, A. M. Cucolo, *Carbon* **2009**, *47*, 1074.
[51] R. G. Forbes, J. H. B. Deane, *Proc. R. Soc. A* **2007**, *463*, 2907.
[52] R. G. Forbes, *J. Appl. Phys.* **2016**, *120*, 054302.
[53] C. J. Edgcombe, *Phys. Rev. B* **2005**, *72*, 045420.
[54] Y. S. Ang, S.-J. Liang, L. K. Ang, *MRS Bull.* **2017**, *42*, 505.
[55] C. Kim, Y. S. Choi, S. M. Lee, J. T. Park, B. Kim, Y. H. Lee, *J. Am. Chem. Soc.* **2002**, *124*, 9906.
[56] A. Di Bartolomeo, M. Passacantando, G. Niu, V. Schlykow, G. Lupina, F. Giubileo, T. Schroeder, *Nanotechnology* **2016**, *27*, 485707.
[57] L. Jiang, P. Liu, L. Zhang, C. Liu, L. Zhang, S. Fan, *RSC Adv.* **2018**, *8*, 31830.
[58] V. I. Kleshch, A. A. Tonkikh, S. A. Malykhin, E. V. Redekop, A. S. Orekhov, A. L. Chuvilin, E. D. Obraztsova, A. N. Obraztsov, *Appl. Phys. Lett.* **2016**, *109*, 143112.
[59] A. Di Bartolomeo, A. Scarfato, F. Giubileo, F. Bobba, M. Biasiucci, A. M. Cucolo, S. Santucci, M. Passacantando, *Carbon* **2007**, *45*, 2957.
[60] F. Giubileo, A. Di Bartolomeo, M. Sarno, C. Altavilla, S. Santandrea, P. Ciambelli, A. M. Cucolo, *Carbon* **2012**, *50*, 163.
[61] R. Bhattacharya, M. Turchetti, P. D. Keathley, K. K. Berggren, J. Browning, *J. Vac. Sci. Technol., B* **2021**, *39*, 053201.

© 2022 The Authors. Advanced Electronic Materials published by Wiley-VCH GmbH

2199160x, 2023, 1, Downloaded from https://onlinelibrary.wiley.com/doi/10.1002/aelm.202200690 by Universita Di Salerno, Wiley Online Library on [10/01/2023]. See the Terms and Conditions (https://onlinelibrary.wiley.com/terms-and-conditions) on Wiley Online Library for rules of use; OA articles are governed by the applicable Creative Commons License